CRYSTAL GROWTH & DESIGN

pubs.acs.org/crystal

Article

Syntheses, Structures, and Magnetic Properties of Novel [3×1 + 2×1] Pentanuclear Zinc(II)-Lanthanide(III) Cocrystal Complexes: Slow Magnetic Relaxation Behavior of the Dy(III) Analogue

Published as part of a Crystal Growth and Design virtual special issue on Molecular Magnets and Switchable Magnetic Materials

Soumalya Roy, Jiyuan Du, Ezhava Manu Manohar, Tarik Aziz, Tapan K. Pal,* Lin Sun,* Naushad Ahmed,* and Sourav Das*

Cite This: *Cryst. Growth Des.* 2023, 23, 2218−2230

Read Online

ACCESS | Metrics & More | Article Recommendations | Supporting Information

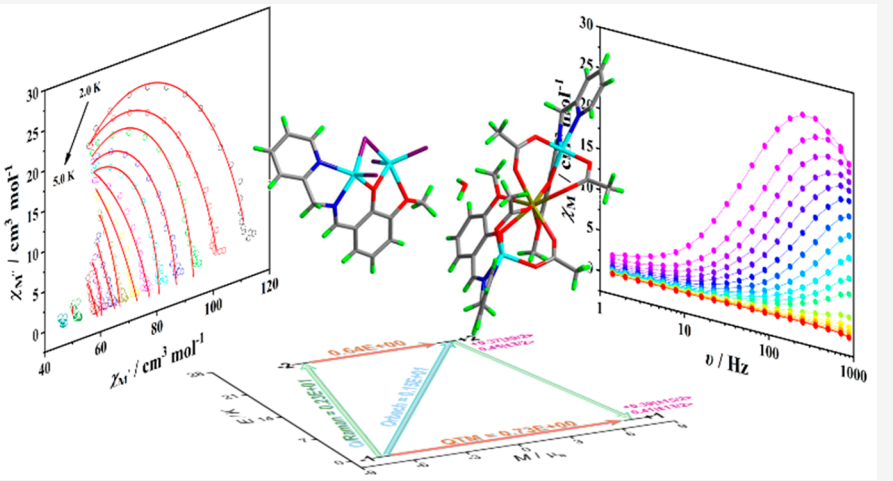

ABSTRACT: A new family of 3d-4f polynuclear cocrystals $[LnZn_2L_2(CH_3CO_2)_4]\cdot[Zn_2Cl_4L]\cdot H_2O$ [where Ln^{III} = Gd(**1**), Tb(**2**), and Dy(**3**)] are synthesized by the sequential reaction of a tetradentate multisite coordinating compartmental ligand, i.e., (*E*)-2-methoxy-6-(((pyridine-2-ylmethyl)imino)methyl)phenol, in the presence of $LnCl_3\cdot 6H_2O$ and $Zn(OAc)_2\cdot 2H_2O$. The detailed studies involve mainly synthesis, structure, and magnetic properties of three isostructural cocrystals. The X-ray diffraction analysis reveals that complexes **1**−**3** crystallize in triclinic crystal system with the $P\bar{1}$ space group. The dimeric $[Zn_2Cl_4L]^-$ complex appears as a cocrystal in the vicinity of the $[LnZn_2L_2(CH_3CO_2)_4]^+$ crystal structure to counter balance the overall charge on the primary coordination sphere. Magnetic relaxation studies indicate that zero-field out-of-phase magnetic susceptibility signals are observed only for complex **3** (Dy^{III} analogue) which gets well resolved in the presence of a H_{dc} = 0.5 kOe magnetic field. The extracted effective energy barrier (U_{eff}) and pre-exponential factor (τ_0) for **3** is found to be 13.53 K and 1.78 × 10^{-6} s, respectively. The appearance of single-ion magnet properties for **3** is rationalized with CASSCF/SO-RASSI/SINGLE_ANISO based *ab initio* calculations.

INTRODUCTION

The construction of novel crystalline solids with necessary intriguing physiochemical characteristics is highly reliant on developing, comprehending, and rationalizing the intra- to intermolecular interactions in the context of crystal packing.[1−5] In real scenarios, identical molecular units form oligomers or an extended network through intermolecular interactions.[6−8] Consequently, intermolecular interactions between distinct molecular components at a definite stoichiometric ratio can lead to the development of crystalline adducts or multi-component crystals called cocrystals.[9−21] Cocrystallization of two separate molecules is undeniably a method to deliberately

Received: October 31, 2022
Revised: February 10, 2023
Published: February 27, 2023

https://doi.org/10.1021/acs.cgd.2c01256
Cryst. Growth Des. 2023, 23, 2218−2230

influence the position of molecules in the crystal lattice, which might affect the possibilities of improving material performance for applications.[22−32] For instance, pharmaceutical cocrystals can enhance the dissolution rate and bioavailability of an active pharmaceutical ingredient (API) without changing its native structure.[33−44] Moreover, the cocrystallization technique of energetic materials such as 2,4,6-trinitrotoluene (TNT) can boost the explosive intensity of the substance.[45−49] Furthermore, molecular cocrystals can also exhibit other physiochemical properties such as nonlinear optical, ferroelectric, dielectric, and charge-transfer properties, making them more appealing to the scientific community.[50−55] Until now, because of the rational understanding of supramolecular noncovalent interactions, reports on cocrystals mainly involve organic systems, particularly those with acid−base pairs and pharmaceutical molecules.[56−59] Although inorganic−organic cocrystals do exist, cocrystals with distinct metal complexes are limited. The fundamental reason for this is that metal complexes with different coordination environments rarely have the same potential energy for lattice packing and crystallization kinetics.[60−67] However, various other parameters that directly impact cocrystal processing include good ligand design, a suitable solvent ratio, temperature, and proper stoichiometric and enantiomeric ratios. Although some transition metal-based cocrystals were reported in the literature, cocrystals comprising 4f metal ions or 3d-4f metal ions are exceedingly rare. Liu and co-workers have reported the first 4f-based tetranuclear metallocage and mononuclear Dy^{III} cocrystal complex.[68] Das and co-workers have also reported 4f based cocrystals containing a spirocyclic pentanuclear cationic lanthanide (Ln) unit and one mononuclear anionic lanthanide unit [Ln^{III} = Dy^{III} and Tb^{III}].[69] Zhang and co-workers have reported the first genuine 3d-4f cocrystal of a mononuclear Dy^{III} complex with a square-planar Cu^{II} complex consisting of only one reactant.[70] In fact, the field of lanthanide coordination chemistry has gained a lot of attention because of its potential applications in catalysts, photoluminescent materials, and molecular magnetic materials.[71−89] Compounds containing lanthanide (Ln) ions are of special interest in the field of molecular magnetism because they may exhibit an extraordinary slow relaxation of magnetization behavior or single molecule/ion magnet (SMM/SIM) behavior arising from the large spin and significant magnetic anisotropy of Ln^{III} ions.[90−99] Despite substantial progress in the field of SMMs, it is worth mentioning that QTM-induced relaxation processes are the biggest roadblock in lowering the effective energy barrier (U_{eff}) of lanthanide-containing SMM complexes.[98,100−106] There are a few strategies to mitigate the QTM, such as ligand fields of high symmetries around the lanthanide ions, application of a tiny static magnetic field, dilution of such complexes in a diamagnetic matrix, or a strong superinteraction among the paramagnetic ions (3d and 4f metal ions).[92,107−113] However, a review of the literature has shown that magnetic exchange coupling resulting from 3d/4f metal ions is often weak and has a small effective energy barrier, but when paramagnetic 3d ions are replaced by diamagnetic metal ions, it may offer magnetic dilution to the system, slowing the QTM process and elevating the energy barrier.[114,115] Furthermore, recent studies revealed that the presence of diamagnetic coordinating ions in a Dy^{III} system can alter the electron density distribution around the Dy^{III} ion (particularly around the bridging phenoxido oxygen donor), influencing the orientation of the Dy^{III} g tensor and therefore increasing the energy barrier.[116−119]

Based on our research backgrounds and motivated by the above-mentioned discussion, in this study, we have attempted to construct a distinct type of polynuclear Zn^{II}-Ln^{III} complex utilizing a tridentate Schiff base ligand (*E*)-2-methoxy-6-(((pyridine-2-ylmethyl)imino)methyl)phenol in the presence of $Zn(OAc)_2{\cdot}2H_2O$ and $LnCl_3{\cdot}6H_2O$ [Ln^{III} = Gd^{III}, Tb^{II}, and Dy^{III}], which allows an assembly of cocrystals having a general formula $[LnZn_2L_2(CH_3CO_2)_4]{\cdot}[Zn_2Cl_4L]{\cdot}H_2O$ [Ln = Gd^{III}, Tb^{III}, and Dy^{III}]. According to the CCDC database, this is the first ever report of 3d-4f and 3d cocrystals based on a Zn^{II}-Ln^{III} system, and hereby, we report the syntheses, structural properties, and magnetic behavior of $[LnZn_2L_2(CH_3CO_2)_4]{\cdot}[Zn_2Cl_4L]{\cdot}H_2O$ [Ln^{III} = Gd^{III}(**1**), Tb^{III}(**2**), and Dy^{III} (**3**)].

EXPERIMENTAL SECTION

Experimental Section. *Materials and Methods.* All chemicals, solvents, and reagents were purchased from commercial sources and were used without further purification. *o*-Vanillin (99%, 148-53-8), 2-picolylamine (99%, 3737-51-9), $DyCl_3{\cdot}6H_2O$ (99.99%, 15059-52-6), and $Zn(OAc)_2{\cdot}2H_2O$ (99.99%, 557-34-6) were obtained from Sigma-Aldrich Chemical Co (USA). Solvents were reagent grade and distilled under nitrogen prior to their use. All other chemicals were reagent grade, available commercially, and used as received. IR data were collected in the range of 450−4500 cm^{-1} using a PerkinElmer Spectrum two FTIR spectrometer with an ATR module. Elemental analysis was done using a Carlo Erba EA 1108 analyzer. The Thermoquest CE instrument CHNS-O, EA/110 model was employed for elemental analysis. The thermal stability of the complexes, i.e., thermogravimetric analysis (TGA), was assessed by a TA Instruments Q 600 device. The phase purity of the polycrystalline samples was confirmed by obtaining the powder X-ray diffraction data at room temperature on a Bruker AXS D8 advanced diffractometer using CuKα radiation (λ = 1.5418 Å) across the 2θ range from 5 to 50°. All the samples were analyzed using an inductively coupled plasma optical emission spectrometer (Thermo Fischer Scientific, Magnetic sector, ICPMS, IIT Powai). Single crystal X-ray data of compounds **1**−**3** were collected from a Bruker Kappa APEXII diffractometer having graphite-monochromatic with MoKα radiation (λ = 0.71073 Å). The structure was solved by the software packages SMART and SAINT,[120] SADABS,[121] SHELXTL[122,123] and refined by the full-matrix least-squares of F^2 using the SHELXL-2014[124] along with Olex-2 software.[125] Anisotropic thermal parameters were assigned to all non-hydrogen atoms. Diamond 3.1e software[126] was used to design the crystal structure. The CCDC numbers of complexes **1**−**3** are 2216581 (for **1**), 2216586 (for **2**), and 2216591 (for **3**) respectively and can be obtained from www.ccdc.cam.ac.uk/data_request/cif. The crystallographic data and parameters are presented in Table S1. Magnetic measurements were performed in the temperature range 2 K−300 K with an applied field of 1000 Oe, using a Quantum Design MPMS-XL-7 SQUID magnetometer on polycrystalline samples. The diamagnetic corrections for compounds were estimated using Pascal's constants. Alternating current (ac) susceptibility experiments were performed using an oscillating ac field of 2.0 Oe at ac frequencies ranging from 1 to 1000 Hz. The magnetization was measured in the field range 0−7 T. The diamagnetic corrections were calculated from Pascal's constants. For computational studies on complex **3**, we have chosen CAS (9, 7) *ab initio* calculations using the MOLCAS 8.2 suite.

Synthesis of LH. The pyridine moiety based Schiff based ligand (LH) was synthesized by the condensation reaction of *o*-vanillin with 2-picolylamine at 70 °C.[127−130]

Synthesis of 1−*3.* The ligand LH was dissolved in MeOH/MeCN solvent and stirred followed by the addition of $DyCl_3{\cdot}6H_2O$, and 30 min later, $Zn(OAc)_2{\cdot}2H_2O$ was added to the reaction mixture and then NaOH base was added in a 1:1:1:2 stoichiometric ratio, and again stirred for a period of 16 h at room temperature. After that, the reaction mixture was filtered out, and the precipitate was dissolved in MeOH/MeCN. Good quality yellow colored block-shaped crystal was obtained by slow evaporation and was appropriate for single crystal XRD. The

https://doi.org/10.1021/acs.cgd.2c01256
Cryst. Growth Des. 2023, 23, 2218−2230

Scheme 1. General Synthetic Route to Isolate 1−3

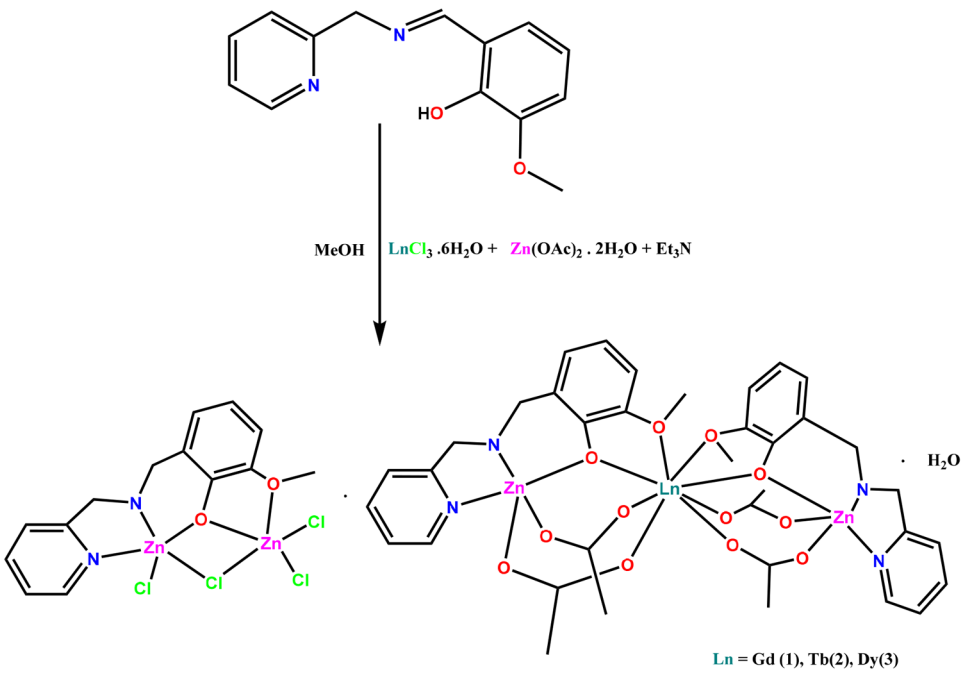

specific amount of each complex and characterization data is given below.

[GdZn$_2$L$_2$(CH$_3$CO$_2$)$_4$]·[Zn$_2$Cl$_4$L]·H$_2$O (***1***). Quantities: LH (0.040 g, 0.16 mmol, GdCl$_3$·6H$_2$O 0.062 g, 0.16 mmol, Zn(OAc)$_2$·2H$_2$O (0.036 g, 0.16 mmol), Et$_3$N (0.045 mL, 0.45 mmol). Yield: 0.039 g 30% (based on Gd^{3+}) Anal. Calcd for $C_{50}H_{53}Cl_4GdN_6O_{15}Zn_4$ (1512.74) Cald C, 28.59; H, 3.53; N, 5.56 Found: C, 28.49; H, 3.32, N, 5.69 IR (KBr) (cm^{-1}): 1608.61(s), 1572.52(s), 1519.93(s), 1448.78(s), 1404.44(m), 1368.35(m), 1288.95 (m), 1084.78(m).

[TbZn$_2$L$_2$(CH$_3$CO$_2$)$_4$]·[Zn$_2$Cl$_4$L]·H$_2$O (***2***). Quantities: LH (0.040 g, 0.16 mmol), TbCl$_3$·6H$_2$O (0.062 g, 0.16 mmol), Zn(OAc)$_2$. 2H$_2$O (0.036 g, 0.16 mmol), and Et$_3$N (0.045 mL, 0.45 mmol). Yield: 0.039 g, 36% (based on Tb^{3+}) Anal. Calcd for $C_{50}H_{53}Cl_4N_6O_{15}TbZn_4$ (1535.87): Cald C, 38.98; H, 3.47; N, 5.47 Found: C, 39.07; H, 3.66, N, 5.59; IR (KBr) (cm^{-1}): 1635.42(s), 1545.71(s), 1501.37(s),1475.59(s), 1404.44(s), 1297.20(m), 1226.05(m), 1110.56 (m) 995.07(m)

[DyZn$_2$L$_2$(CH$_3$CO$_2$)$_4$]·[Zn$_2$Cl$_4$L]·H$_2$O (***3***). Quantities: LH (0.040 g, 0.16 mmol), DyCl$_3$·6H$_2$O (0.062 g, 0.16 mmol), Zn(OAc)$_2$·2H$_2$O (0.036 g, 0.16 mmol), Et$_3$N (0.045 mL, 0.45 mmol). Yield: 0.038 g, 34% (based on Dy^{3+}) Anal. Calcd for $C_{50}H_{53}Cl_4DyN_6O_{15}Zn_4$ (1543.82): Calcd C, 38.89; H, 3.47; N, 5.44 Found: C, 40.03; H, 3.36, N, 5.58; IR (KBr) (cm^{-1}): 1599.33(s), 1572.52(s), 1528.18(s), 1421.97(s), 1270.39(m), 1129.12(m), 1084.78(m), 923.92(m).

RESULTS AND DISCUSSION

Synthesis Aspects. Cocrystallization is one of the fascinating wings of crystal engineering that alters the physicochemical properties of the material. In that context, the tridentate Schiff base ligand (LH) possessing a well-defined *N,N,O* potential coordination environment has been previously employed for the synthesis of 3d, 4f, and 3d-4f metal−ligand complexes. The ligand has two definite pockets to hold the metal ions in a μ_2-η^1: η^1: η^2: η^1 binding mode (Figure S3), which is supported by a literature review.[127−130]

LH was used by Powell et al. to assemble linear shaped heterometallic [Zn$_2$Ln$_4$] clusters[127] where the ligand has utilized μ_2-η^1: η^1: η^2: η^1 binding. Wang et al. has utilized LH in a step-by-step and competitive assembly of two Dy(III)-base compound where similar binding mode has been observed.[128]

Utilizing the same ligand system, we report the syntheses of a series of rare heterometallic cocrystals [Zn$_2$Cl$_4$L]·[LnZn$_2$L$_2$(CH$_3$COO)$_4$]·H$_2$O [Ln^{III} = Gd^{III} (**1**), Tb^{III} (**2**), and Dy^{III} (**3**)].

Single-crystal X-ray diffraction (SCXRD) study of all the complexes (**1**−**3**) disclosed that all these compounds are crystallized in the *triclinic* crystal system and $P\bar{1}$ space group. We have taken the representative complex **1** for the crystal structure description of all. The selected bond distances and bond angles are given in the Supporting Information (Tables S2−S4). The asymmetric unit of **1** is depicted in Figure 1, while the asymmetric unit structure of **2** and **3** is presented in the Supporting Information (Figure S1 and Figure S2). The asymmetric unit of **1** is electronically neutral, and a total of 11

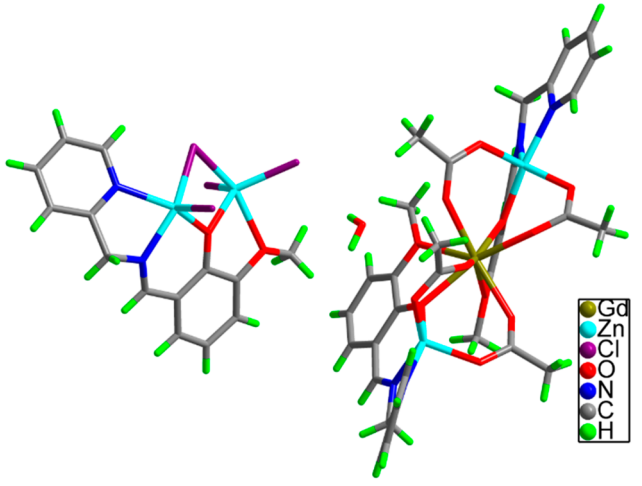

Figure 1. Perspective view of the crystal structure of complex **1** present in the asymmetric unit (ASU).

https://doi.org/10.1021/acs.cgd.2c01256
Cryst. Growth Des. 2023, 23, 2218−2230

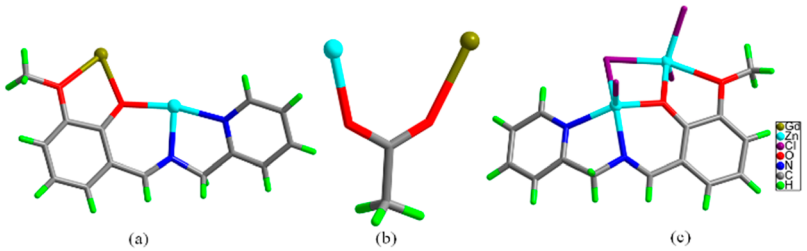

Figure 2. (a, b, c) Presentation of the binding fashion of the main ligand, coligand (acetate ion), and main ligand respectively in complex **1**.

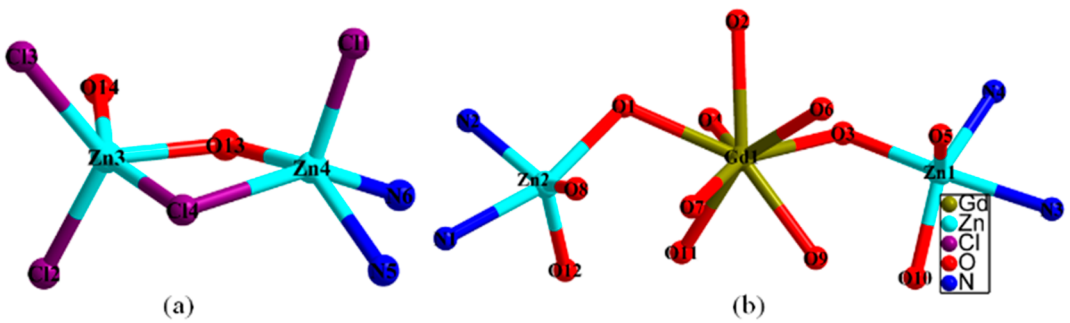

Figure 3. (a, b) The anionic binuclear $[Zn_2O_2N_2Cl_4]^-$ and trinuclear cationic $[Zn_2GdO_{12}N_4]^+$ clusters respectively in **1**.

cationic charges from the crystallographically independent metal ions (four Zn^{2+} and one Gd^{3+}, all are full occupancy) are balanced by the three anionic charges from the three deprotonated main ligands (L^-), four anionic charges from four chloride ions, and four anionic charges from four acetate (OAc) ligand. Interestingly, the structure of **1** and all complexes **2**−**3** consists of a binuclear anionic $[Zn_2LCl_4]^-$ unit as a cocrystal and a trinuclear cationic $[Zn_2GdL_2(Ac)_4]^+$ unit (Figure 1). In addition, one water molecule is crystallizing between the two units (Figure 1).

From the design perspective of the ligand network of HL, it is clear that it contains two different pockets for a metal ion binding site (Figure S3). The pocket A consists of 2N and one O as a metal chelating sites. The pocket B has 2O as a metal chelating sites (Figure S3). Remarkably, these pockets are capable of accommodating the metal ions very comfortably, resulting in the formation of a multimetallic clustered architecture. Also, the −OH group present on the benzene ring of the main ligand HL is deprotonated during the reaction to produce phenolate oxygen, which holds the metal ions very strongly through μ_2 fashion. A close inspection of the crystal structure of **1** revealed that the discrete cocrystallized trinuclear cationic counterpart of **1** is constructed from two deprotonated main ligand (L^-), four OAc anions as a coligand, two Zn^{2+} ions, and one Gd^{3+} ion. The binding fashion of the main ligand and the coligand in this cationic counterpart is presented in Figure 2a. Each ligand binds to the two metal ions (Zn^{2+} and Gd^{3+}) through η^1-nitrogen, η^1-nitrogen, η^2-oxygen and η^1-oxygen, i.e. μ_2-η^1: η^1: η^2: η^1, and each Ac anion is binding to two metal ions (Zn^{2+} and Gd^{3+}) through a *syn-syn* bidentate bridging mode (μ_2-η^1: η^1) (Figure 2b).

These coordination modes lead to the formation of a linear trimeric metal cluster of formula $[Zn_2GdO_{12}N_4]^+$ where Gd^{3+} ion is occupying the central position of the core, and the two Zn^{2+} ions are at the extreme end of the trimeric core (Figure 3b). The analogous anionic binuclear $[Zn_2O_2N_2Cl_4]^-$ and trinuclear cationic $[Zn_2MO_{12}N_4]^+$ clusters also exist in another two cocrystals (Zn^{II}−Tb^{III} and Zn^{II}−Dy^{III}) (Figures S4 and S5). A point to be noted here is that the high oxophilic character of gadolinium renders a greater number of oxygen anions to get attached with the gadolinium in this trinuclear core. The coordination number of Gd1, Zn1/Zn2 are eight and five respectively. These coordination numbers are fulfilled by 8O for Gd1 and 3O, 2N for both $Zn^{II}1$ and $Zn^{II}2$, leading to the building of a distorted square antiprismatic geometry for Gd^{III} and distorted trigonal bipyramidal geometry for both the Zn^{II} ions (Figure 4).

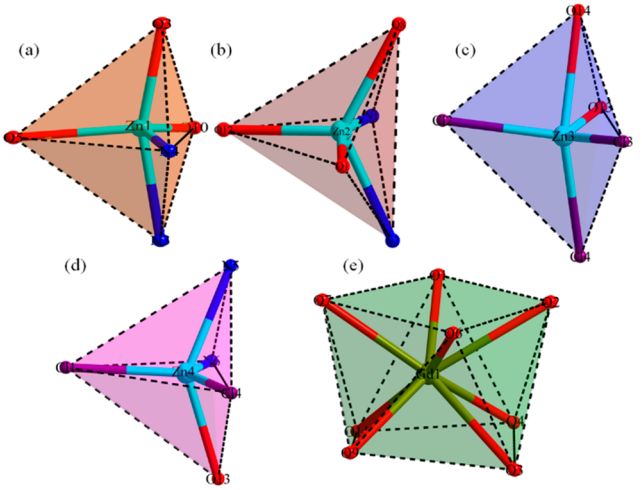

Figure 4. (a−e) The representation of coordination environment around Zn1, Zn2, Zn3, Zn4, and Gd1 metal ions in **1**.

On the other hand, another cocrystallized anionic binuclear discrete unit, $[Zn_2LCl_4]^-$, contains two Zn^{2+} ions (full occupancy), one deprotonated main ligand (L^-), and four chloride (Cl^-) ions (Figure 1). The main ligand binds to the two Zn^{2+} ions through η^1-nitrogen, η^1-nitrogen, η^2-oxygen, and η^1-oxygen, i.e., μ_2-η^1: η^1: η^2: η^1. Out of four Cl^- ions, three Cl^- ions are attached to the two Zn^{2+} ions through η^1 fashion, and a

https://doi.org/10.1021/acs.cgd.2c01256
Cryst. Growth Des. 2023, 23, 2218−2230

fourth Cl^- ion binds to both the Zn^{2+} ions via a η^2 manner (μ_2-η^2) (Figure 2c). These binding patterns of both the main ligand and chloride ions afforded bimetallic metallic clusters of formula $[Zn_2O_2N_2Cl_4]^-$ (Figure 3a). The coordination number of both the Zn^{2+} ions (Zn3 and Zn4) is five, which are obtained from 3Cl, 2O for Zn3 and 1O, 2N, and 2Cl for Zn4, giving rise to trigonal bipyramidal and square pyramidal geometry for Zn3 and Zn4 respectively (Figure 4). The coordination number and coordination environment around the respective metal ions in other two cocyrstals are displayed in Figures S6 and S7. The metric parameters of the current case are comparable to the same core found in the literature and are briefed in Table S9.

It is worth mentioning that the synthesis and stabilization of the cocrystal involves the suitable noncovalent supramolecular interaction between two or more components in their solid state and that allows their perfect atomistical orientation in the cocrystal network. In **1**, the two components viz. cationic and ionic parts displayed the various noncovalent interactions (C−H···π, π ··π, and hydrogen bonding) in the crystallographic network (Figure 5 and Table 1). As per our speculation, the

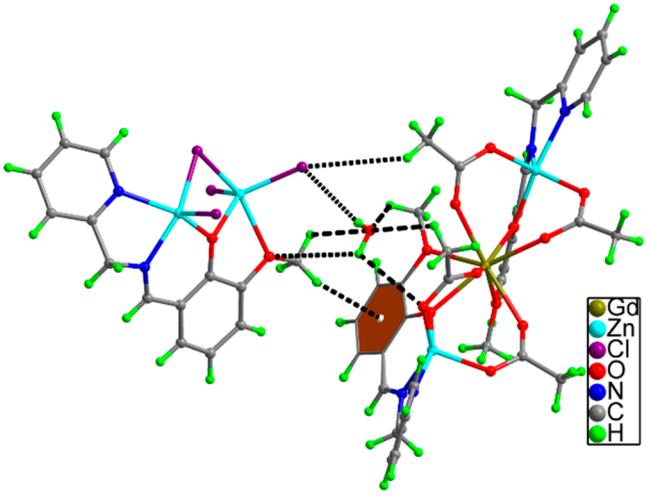

Figure 5. Existence of noncovalent interaction in **1**.

Table 1. Various Possible Interaction Parameters for Complex 1 (Zn−Gd)

components	bond distance (Å)	bond angle (deg)
C37−H37B·····π	2.637(1)	142.497(7)
O15−H15E·····Cl3	2.653(3)	109.545(7)
C15−H15B·····O15	3.280(1)	102.729(7)
C37−H37C·····O15	3.073(1)	101.990(8)
O15−H15D·····O14	3.191(8)	108.809(4)
C36−H36B·····Cl3	3.580(3)	124.568(7)
O15−H15D·····O10	3.369(7)	108.736(1)
C34−H34C·····O15	3.848(1)	113.703(8)

presence of water molecules between the two discrete ionic units helps to bring them close together and stabilize them through noncovalent interactions (Figure 5). The similar noncovalent supramolecular interactions are also present in other two cocrystals (ZnTb and ZnDy) (Figures S8−S9 and Tables S5−S6).

The phase purity of polycrystalline samples of complexes **1**, **2**, and **3** was confirmed by the powder X-ray diffraction method. As given in Figure S11, the experimental PXRD patterns are in good agreement with the simulated patterns generated from their single crystal X-ray diffraction data for complexes **1**, **2**, and **3**.

The thermogravimetric analysis (TGA) has been employed to check the thermal stability of complexes **1**−**3**. The TGA studies reveal that all the complexes **1**−**3** have a similar pattern of TGA, and all complexes are stable up 250 °C as weight losses are negligible up to this temperature. Above 350 °C, rapid loss validated the disintegration of these complexes (Figure S12).

An ICP-MS analysis was conducted on the powder sample of **1**, **2**, and **3** respectively for the elemental analysis, and the results show that the calculated values correspond with the mass percentages obtained practically. The ICP calculation details are provided in Supporting Informatiomn.

Hirshfeld Surface Analysis on 1−3. The past few years witnessed investigations on the role of intermolecular interactions with counterions and/or solvent molecules to modulate the dynamic magnetic behavior of metal complexes.[131] In a majority of the cases, the experimental effective energy barrier (U_{eff}) for spin reversal was found to be much lower compared to the calculated (U_{cal}) one. Investigations revealed that intermolecular interactions may trigger the under barrier magnetic relaxation such as Raman and QTM processes. The Hirshfeld surface analysis proves to be a useful tool to determine qualitatively and quantitatively the intermolecular interactions through hydrogen bonding/short contacts and the stability of crystal. We have calculated and analyzed the Hirshfeld surface using CrystalExplorer 21.5 software[132] for all the complexes **1**−**3**. We have mapped calculated Hirshfeld surfaces in d_{norm} 3D plots along with 2D fingerprints (Figure 6 and Figures S13−S16). Here d_e and d_i represent the nearest distance of a molecule from outside and inside of the Hirshfeld surface respectively. In all the cases **1**−**3** the major 50−60% intermolecular interactions are found to be through H···H, while 14−16% of interactions are through H···O/O···H contacts. Other weak interactions such as π−π/CH-π can be analyzed through different views (shape index, curvedness etc.) of Hirshfeld surfaces. The obtained asphericity parameter in the range of 0.136−0.138 indicates highly structural anisotropy present in these metal complexes **1**−**3**.

Magnetic Properties of 1−3. The direct-current (dc) magnetic susceptibility measurements of polycrystalline sample **1**−**3** have been performed in the temperature range of 2 to 300 K, employing an applied field of 1 kOe (Figure 8). At 300 K, the experimental $\chi_M T$ values are 8.06 $cm^3 \cdot K \cdot mol^{-1}$ for **1**, 11.96 $cm^3 \cdot K \cdot mol^{-1}$ for **2**, and 14.32 $cm^3 \cdot K \cdot mol^{-1}$ for **3** respectively, which are close to the expected value of one uncoupled Ln^{III} ion (7.88 $cm^3 \cdot K \cdot mol^{-1}$, $^8S_{7/2}$, $S = 7/2$, $g = 2$ for **1**, 11.81 $cm^3 \cdot K \cdot mol^{-1}$, $^7F_6$, $S = 3$, $L = 3$, $g = 3/2$ for **2** and 14.17 $cm^3 \cdot K \cdot mol^{-1}$, $^6H_{15/2}$, $S = 5/2$, $L = 5$, $g = 4/3$ for **3**). In the case of **1**, as the temperature drops, the $\chi_M T$ values found to be almost constant down to 15 K and then decrease dramatically to reach the lowest $\chi_M T$ value of 7.61 $cm^3 \cdot K \cdot mol^{-1}$ at 2 K. The sudden downtrend can be put down to the presence of weak antiferromagnetic coupling between Gd^{III} ions and/or zero-field splitting (ZFS) effects of the Gd^{III} ions.[133−135]

We have fitted the magnetic susceptibility and magnetization data simultaneously for complex **1** using the PHI program. The best fit yielded $D = +0.21$ cm^{-1}, $g_{Gd} = 2.035$, $zJ = -0.0075$ cm^{-1}. The magnetic anisotropy in the case of complex **1** results from the structural anisotropy as indicated from the asphericity value of 0.138 during Hirshfeld surface analysis.

The values of $\chi_M T$ for **2** and **3** decrease slowly from 300 to 100 K, which were followed by a sharp drop, reaching minimum

https://doi.org/10.1021/acs.cgd.2c01256
Cryst. Growth Des. 2023, 23, 2218−2230

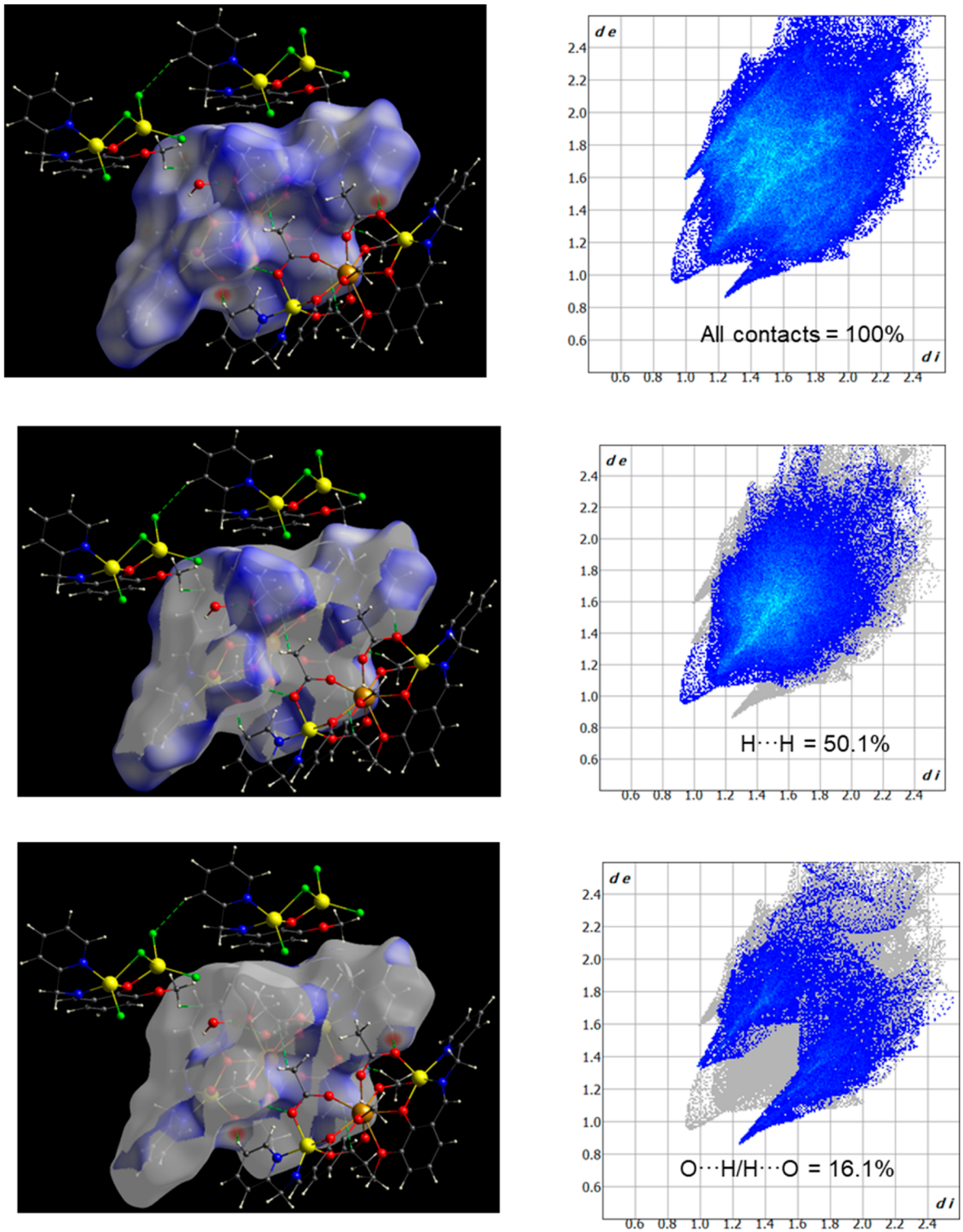

Figure 6. Hirshfeld surface mapped in 3D d_{norm} surface plots (left) and the major intermolecular interactions (right) shown by 2D fingerprint plots for complex **3**. The interactions through H-bonding shown in green dotted lines. The white area represents contacts with lengths equivalent to the sum of the Van der Waals radii of the interacting atoms.

values of 6.18 $cm^3 \cdot K \cdot mol^{-1}$ for **2** and 10.85 $cm^3 \cdot K \cdot mol^{-1}$ for **3** at 2 K, respectively. This typical decrease may be attributed to the thermal depopulation of the Stark sublevels of Ln^{III} ions in **2** and **3**.

The magnetization measurements for **1**−**3** have been performed at different temperatures in an applied field varying from 0 to 70 kOe (Figure 9). For **1**, the magnetization value increases with increasing magnetic field up to 20 kOe field and slowly reaches a saturation value of 7.18 Nμ_B at 70 kOe, which is close to the theoretical value of single Gd^{III} ions (7 Nμ_B). The declined magnetization data illustrate that the curves experience magnetic saturation, all of which are superimposed onto a single

https://doi.org/10.1021/acs.cgd.2c01256
Cryst. Growth Des. 2023, 23, 2218−2230

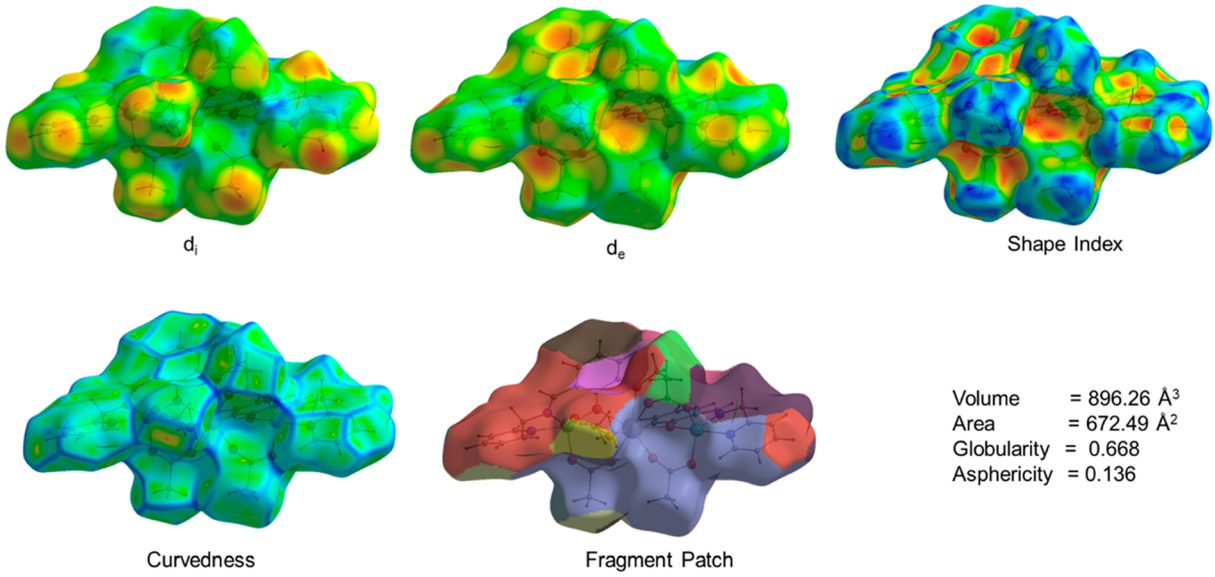

Figure 7. Different views of Hirshfeld surfaces for **3** indicating the presence of weak intermolecular interactions.

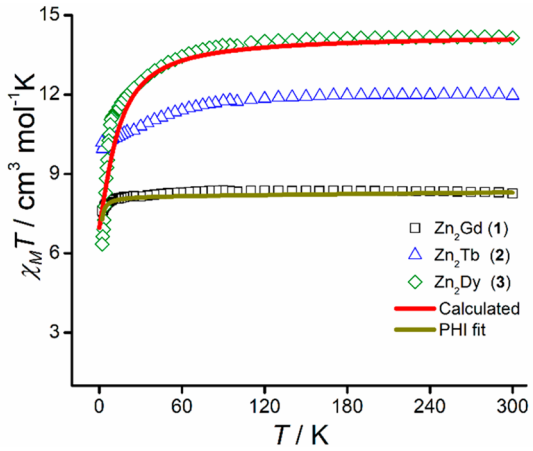

Figure 8. $\chi_M T$ versus T plots for **1**−**3** at 1 kOe.

master curve, suggesting that the isotropy of Gd^{III} ions exists.[136] However, for **2** and **3**, the magnetization values are 6.25 Nμ_B and 7.41 Nμ_B at 2 K and 70 kOe, which are away from the theoretical saturation values of one independent Dy^{III} ions (10 Nμ_B) and one independent Tb^{III} ions (9 Nμ_B). Such a deviation can be ascribed to the existence of magnetic anisotropy in two complexes and/or low-lying excited states.[137,138] Meanwhile, non-superimposed M versus H/T curves at 2 K, 3 and 5 K can be observed, which further confirms the presence significant magnetic anisotropy[139] (Figure 9).

To achieve a better understanding of dynamic magnetic properties of **1**−**3**, the temperature-dependent alternating current (ac) susceptibility values were measured at different frequencies and under a zero field (Figures S17−S19). There is no out-phase (χ_M'') signals of **1** and **2** at zero field. However, the in-phase (χ_M') and out-phase (χ_M'') signals of **3** show a noticeable upturning trend as the temperature declines, implying the existing of the slow magnetic behavior. Notably, no peaks can be observed due to the strong quantum tunnelling of magnetization (QTM) (Figure S19). This is consistent with the observation from the frequency-dependent alternating current (ac) susceptibility measurements of **3**, where no peaks shifts have been observed (Figure S20). Therefore, ac susceptibility measurements have been carried out at 2.0 K and varying dc fields from 0 to 4 kOe for **3** to suppress the QTM. As shown in Figure S21, several obvious χ_M'' peaks can be seen by the application of different dc fields from 0.5 to 3.5 kOe, which means an applied magnetic field can suppress QTM effectively. Therefore, the optimum dc field 0.5 kOe field was chosen to achieve the slowest magnetic relaxation. Under a 0.5 kOe field, the out-phase (χ_M'') signals of **3** shows that this process is temperature-dependent, and it further confirms that **3** exhibits SMM behavior (Figure 10). Meanwhile, fitting of the cole−cole plots with the generalized Debye model (eq 1) yielded α parameters in the range of 0.23−0.18 (Figure 10, Table S8).

$$\chi_s(\omega) = \chi_s + \frac{\chi_T - \chi_s}{1 + (i\omega\tau)^{1-\alpha}} \quad (1)$$

The α value fall in the range of earlier reported SMMs with a relatively wide distribution of the relaxation process suggests the presence of multirelaxation processes in **3**. Further to extract the effective energy barrier of **3**, the Arrhenius plot ($\ln(\tau)$ versus T^{-1}) was constructed (where τ is the relaxation time obtained from a Cole−Cole fit). The slight deviation of the $\ln(\tau)$ versus T^{-1} plot from linearity indicates the presence of other under barrier magnetic relaxations such as Raman and direct processes. We have fitted the Arrhenius plot using the following equation:

$$\frac{1}{\tau} = \frac{1}{\tau_{QTM}} + AH^2T + CT^n + \frac{1}{\tau_0}\left(\frac{-U_{eff}}{K_BT}\right) \quad (2)$$

where the first term of right-hand side denotes the QTM process, the second term denotes a field dependent direct process, the third term denotes the Raman process, and the last term denotes the Orbach process. An excellent fit was observed with the Raman and Orbach process. The effective energy barrier (U_{eff}) for the Orbach process was found to be 13.53 K (τ_0 = 1.78 × 10^{-6} s) along with the Raman (C = 433, n = 2.48) process.

Computational Studies on 3. The observation of experimental magnetic behavior for complexes **2** and **3** suggests

https://doi.org/10.1021/acs.cgd.2c01256
Cryst. Growth Des. 2023, 23, 2218−2230

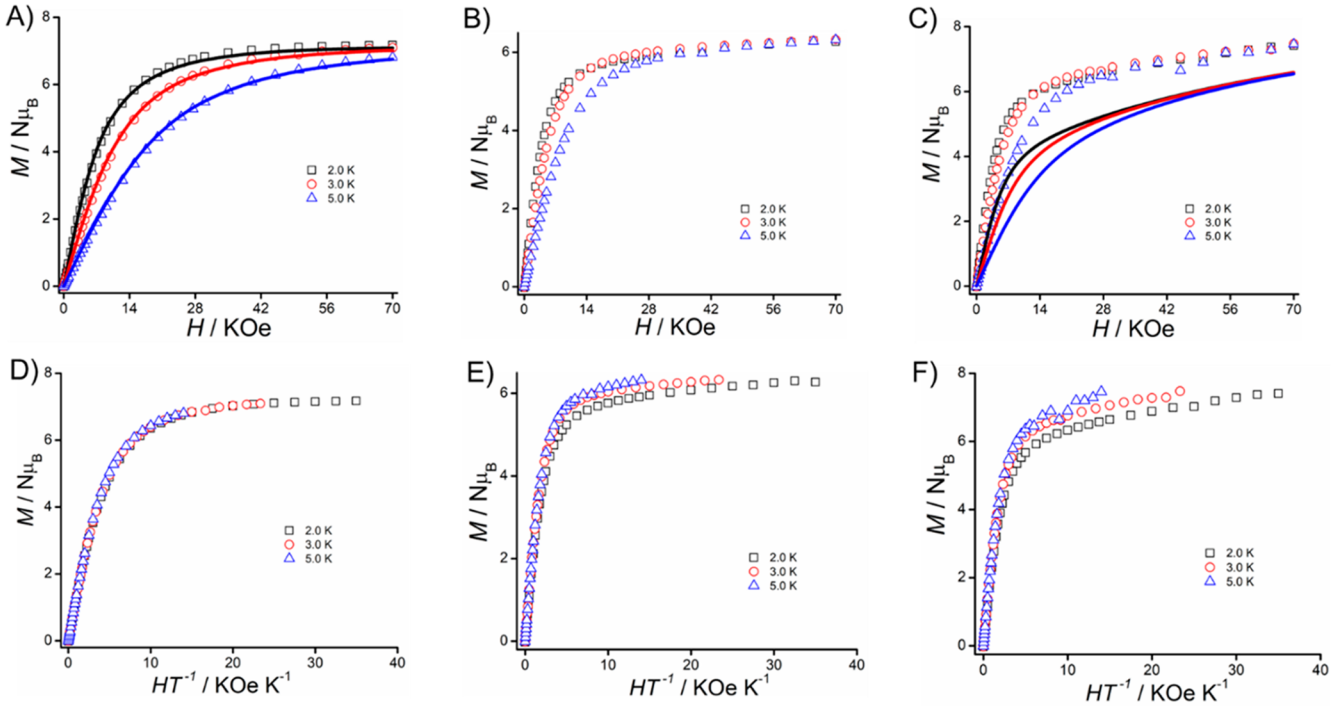

Figure 9. Magnetization (M versus H) and reduced magnetization (M versus HT^{-1}) plots for **1** (panel A and D), for **2** (panel B and E), and for **3** (panel C and F) respectively at the indicated temperatures. The solid lines represent the best fitted data in the case of **1** (panel A) using PHI, while in the case of **3** (panel C) these are *ab initio* computed data using MOLCAS 8.2.

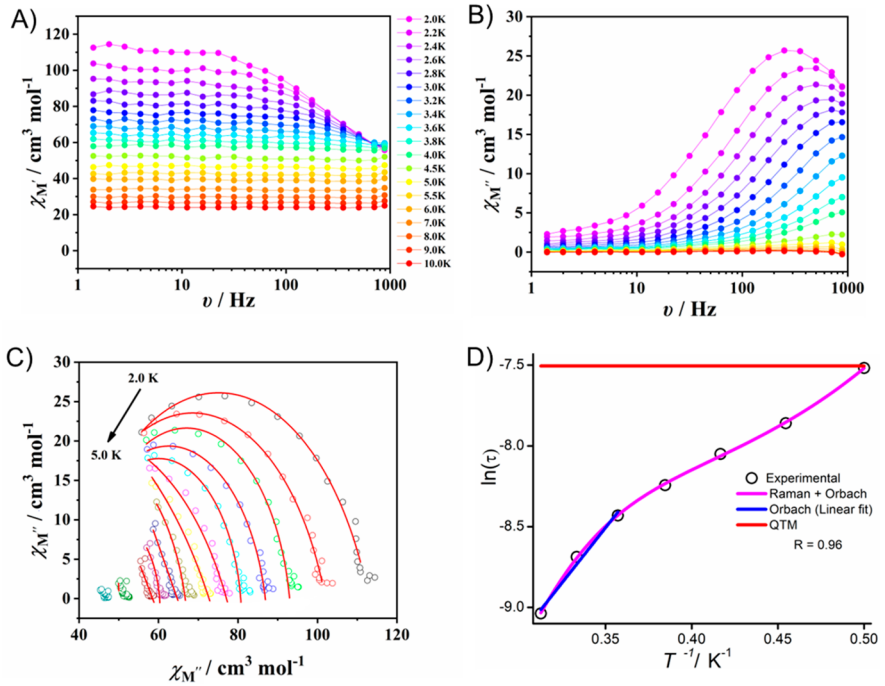

Figure 10. Frequency dependence of the in-phase (A) and out-of-phase (B) ac susceptibility signals under H_{dc} = 0.5 kOe for **3**. Fit of Cole−Cole (C) and ln(τ) vs 1/T (D) plots using a generalized Debye model and Arrhenius law respectively.

that the electronic structure around oblate Tb^{III} and Dy^{III} is not suitable to stabilize the magnetic ground state having the highest ± mJ value in the present ligand environment. To shed light on the observed dynamic magnetic behavior and to get the electronic structure, we have performed CASSCF calculations on the X-ray structures of **3** using the MOLCAS 8.2 suite. In the case of **3**, the obtained g-tensors g_x = 0.7327, g_y = 3.6739, and g_z = 14.4462 clearly suggest that the Dy^{III} ion is very far away from the Ising nature.

The consequence of this can be seen in the energy spectrum (Table S10) of low-lying Kramers' doublets (KD1-KD8) originated from the $^6H_{15/2}$ which does not exceed 418 cm^{-1}

https://doi.org/10.1021/acs.cgd.2c01256
Cryst. Growth Des. 2023, 23, 2218−2230

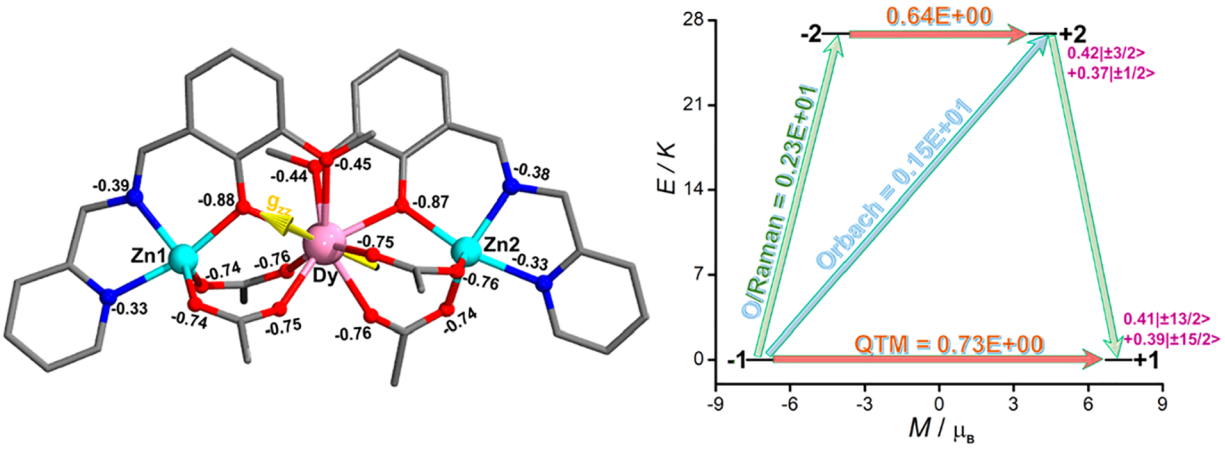

Figure 11. Direction of computed main magnetic axis on Dy^{III} and the predicted magnetic relaxation mechanism in complex **3**. The LoProp charge density shown for the coordinated donor atoms of ligand.

and the first excited state (KD2) found to be located at only 19.19 cm^{-1} from the ground state (KD1). The computed transition magnetic moment value of 0.734 μ_B between ground state KD1 was found to be very high and triggers fast magnetic relaxation from the ground state itself. This theoretical finding rationalized well the experimentally observed non-SMM behavior of **3** under a zero applied field. Further the direction of the main magnetization g_{zz} axis on the Dy^{III} ion was found toward the μ_2-$O_{(phenoxo)}$ bridging ligand which brings the highest charge density (−0.88). To shed light further on the magnetic anisotropy and purity of the ground magnetic state, we have also computed crystal field parameters and wave function decomposition (Table S11). From Table S11 and Figure 11, the present ligand environment stabilizes the ±mJ = 13/2 as ground state with 41% purity and highly admixed with the first excited state ± mJ = 15/2 (39%) and other excited ± mJ states. We have computed crystal field parameters following $\widehat{H_{CF}} = \sum \sum_{k=-q}^{q} B_k^q O_k^q$ Hamiltonian where B_k^q and O_k^q are the crystal field parameters and Stevens' operators respectively. The obtained B_2^q values are given in Table S11. The positive value of $B_2^0 = 0.23 \times 10^{01}$ (while for $B_2^{-2} = -0.20 \times 10^{01}$, $B_2^{-1} = -0.18 \times 10^{01}$, $B_2^1 = -0.13 \times 10^{01}$ and $B_2^2 = 0.38 \times 10^{01}$) leads to a strong deviation from the axial nature and leads to transverse magnetic anisotropy on Dy^{III} in complex **3**. Our theoretical finding is found be well matched with the experimental observations.

CONCLUSIONS

We have utilized a serendipitous approach to self-assemble first Zn^{II}-Ln^{III} based cocrystals by using simple but effective pyridine based tetradentate ligand in the presence of $LnCl_3 \cdot 6H_2O$ [Ln^{III} = Gd(**1**), Tb(**2**), and Dy(**3**)] and $Zn(OAc)_2 \cdot 2H_2O$. The novel Zn^{II}-Ln^{III} based cocrystals are isostructural and consist of an anionic dimeric Zn^{II} unit, a cationic trimeric linear Zn^{II}-Ln^{III}-Zn^{II} unit, and H_2O a solvent of crystallization. As per crystallographic studies, the presence of water molecules between the two discrete ionic units helps to bring them close together and stabilize them through various noncovalent interactions like C−H···π, π ··π, and hydrogen bonding, and these are supported by intermolecular interactions through Hirshfeld surface analysis. In addition, we have also investigated the static and dynamic magnetic behavior of all the complexes. In the series, only Dy^{III} analogues (complex **3**) exhibit field induced SIM behavior with 13.53 K ($\tau_0 = 1.78 \times 10^{-6}$ s) under H_{dc} = 0.5 kOe. We have also rationalized the observed experimental magnetic behavior for **3** through CAS (9, 7) based on *ab initio* theoretical study using MOLCAS 8.2. Furthermore, in the future, we will investigate the compartmental ligand's coordinating adaptability, as it may lead to new complexes with structural diversity and improved magnetic characteristics.

ASSOCIATED CONTENT

Supporting Information

The Supporting Information is available free of charge at https://pubs.acs.org/doi/10.1021/acs.cgd.2c01256.

X-ray crystallography, crystal structure, physical characterization, Hirshfeld surface, magnetic measurements, magnetostructural correlations, results of ab initio investigation, references (PDF)

Accession Codes

CCDC 2216581, 2216586, and 2216591 (complexes **1**−**3**) contain the supplementary crystallographic data for this paper. These data can be obtained free of charge via www.ccdc.cam.ac.uk/data_request/cif, or by emailing data_request@ccdc.cam.ac.uk, or by contacting The Cambridge Crystallographic Data Centre, 12 Union Road, Cambridge CB2 1EZ, UK; fax: +44 1223 336033.

AUTHOR INFORMATION

Corresponding Authors

Tapan K. Pal − *Department of Chemistry, Pandit Deendayal Energy University, Gandhinagar 382426 Gujarat, India*; Email: tapan.pal@sot.pdpu.ac.in

Lin Sun − *Henan Key Laboratory of Polyoxometalate Chemistry, School of Chemistry and Chemical Engineering, Henan University, Kaifeng, Henan 475004, China*; orcid.org/0000-0003-3492-2487; Email: sunlin@vip.henu.edu.cn

Naushad Ahmed − *Department of Chemistry, Indian Institute of Technology Hyderabad, Kandi, Telangana 502285, India*; orcid.org/0000-0002-2671-3581; Email: naushad.chem@gmail.com

Sourav Das − *Department of Basic Sciences, Chemistry Discipline, Institute of Infrastructure Technology Research and Management, Ahmedabad 380026 Gujarat, India*;

https://doi.org/10.1021/acs.cgd.2c01256
Cryst. Growth Des. 2023, 23, 2218−2230

orcid.org/0000-0002-3346-5598; Email: souravdas@iitam.ac.in

Authors

Soumalya Roy − *Department of Basic Sciences, Chemistry Discipline, Institute of Infrastructure Technology Research and Management, Ahmedabad 380026 Gujarat, India*

Jiyuan Du − *Henan Key Laboratory of Polyoxometalate Chemistry, School of Chemistry and Chemical Engineering, Henan University, Kaifeng, Henan 475004, China*

Ezhava Manu Manohar − *Department of Basic Sciences, Chemistry Discipline, Institute of Infrastructure Technology Research and Management, Ahmedabad 380026 Gujarat, India*

Tarik Aziz − *Department of Chemistry, Indian Institution of Technology, Bombay, Powai 400076 Maharashtra, India*

Complete contact information is available at: https://pubs.acs.org/10.1021/acs.cgd.2c01256

Notes

The authors declare no competing financial interest.

■ ACKNOWLEDGMENTS

S.D. acknowledges the financial support from the SERB-DST Early Career Research Award (ECR) with Project Number ECR/2016/001746. L.S. acknowledges financial support from the National Natural Science Foundation of China (22203027) and the Major Project of Science and Technology, Education Department of Henan Province (22A150006). N.A. would like to thank DST-SERB India (File No. PDF/2020/000074) for a postdoctoral fellowship. We are grateful to Mr. Sandip Kundu (Senior Technical Officer, IICB, Kolkata) for providing the single crystal XRD facilities.

■ REFERENCES

(1) Desiraju, G. R. Reflections on the hydrogen bond in crystal engineering. *Cryst. Growth Des.* **2011**, *11* (4), 896−898.
(2) Desiraju, G. R.; Parshall, G. W. *Crystal Engineering: The Design of Organic Solids*; Elsevier, 1989; p *54*.
(3) Bond, A. D. What is a co-crystal? *CrystEngComm* **2007**, *9* (9), 833−834.
(4) Aakeröy, C. B. Crystal engineering: strategies and architectures. *Acta Crystallogr. Sect. B Struct. Sci.* **1997**, *53* (4), 569−586.
(5) Moulton, B.; Zaworotko, M. J. From molecules to crystal engineering: supramolecular isomerism and polymorphism in network solids. *Chem. Rev.* **2001**, *101* (6), 1629−1658.
(6) Matsumoto, N.; Mizuguchi, Y.; Mago, G.; Eguchi, S.; Miyasaka, H.; Nakashima, T.; Tuchagues, J. P. Proton-Dependent Monomer-Oligomer Interconversion of Metal Complexes. *Angew. Chem., Int. Ed.* **1997**, *36* (17), 1860−1862.
(7) Swiegers, G. F.; Malefetse, T. J. New self-assembled structural motifs in coordination chemistry. *Chem. Rev.* **2000**, *100* (9), 3483−3538.
(8) Quiroga, A. G.; Ranninger, C. N. Contribution to the SAR field of metallated and coordination complexes: Studies of the palladium and platinum derivatives with selected thiosemicarbazones as antitumoral drugs. *Coord. Chem. Rev.* **2004**, *248* (1−2), 119−133.
(9) Aitipamula, S.; Chow, P. S.; Tan, R. B. Polymorphism in cocrystals: a review and assessment of its significance. *CrystEngComm* **2014**, *16* (17), 3451−3465.
(10) Desiraju, G. R. Crystal engineering: from molecule to crystal. *J. Am. Chem. Soc.* **2013**, *135* (27), 9952−9967.
(11) Mir, N. A.; Dubey, R.; Desiraju, G. R. Strategy and methodology in the synthesis of multicomponent molecular solids: The quest for higher cocrystals. *Acc. Chem. Res.* **2019**, *52* (8), 2210−2220.
(12) Aitipamula, S.; Banerjee, R.; Bansal, A. K.; Biradha, K.; Cheney, M. L.; Choudhury, A. R.; Desiraju, G. R.; Dikundwar, A. G.; Dubey, R.; Duggirala, N. Polymorphs, salts, and cocrystals: what's in a name? *Cryst. Growth Des.* **2012**, *12* (5), 2147−2152.
(13) Tothadi, S.; Mukherjee, A.; Desiraju, G. R. Shape and size mimicry in the design of ternary molecular solids: towards a robust strategy for crystal engineering. *ChemComm* **2011**, *47* (44), 12080−12082.
(14) Dabros, M.; Emery, P. R.; Thalladi, V. R. A Supramolecular Approach to Organic Alloys: Cocrystals and Three-and Four-Component Solid Solutions of 1, 4-Diazabicyclo [2.2. 2] octane and 4-X-Phenols (X= Cl, CH3, Br). *Angew. Chem., Int. Ed.* **2007**, *46* (22), 4132−4135.
(15) Braga, D.; Grepioni, F.; Maini, L. The growing world of crystal forms. *ChemComm* **2010**, *46* (34), 6232−6242.
(16) Etter, M. C. Encoding and decoding hydrogen-bond patterns of organic compounds. *Acc. Chem. Res.* **1990**, *23* (4), 120−126.
(17) Aakeröy, C. B.; Beatty, A. M.; Helfrich, B. A. Total synthesis" supramolecular style: Design and hydrogen-bond-directed assembly of ternary supermolecules. *Angew. Chem., Int. Ed.* **2001**, *40* (17), 3240−3242.
(18) Urbanus, J.; Roelands, C. M.; Verdoes, D.; Jansens, P. J.; ter Horst, J. H. Co-crystallization as a separation technology: controlling product concentrations by co-crystals. *Cryst. Growth Des.* **2010**, *10* (3), 1171−1179.
(19) Jana, A.; Mohanta, S. A tale of crystal engineering of metal complexes derived from a special ligand family having a cosmopolitan compartment. *CrystEngComm* **2014**, *16* (25), 5494−5515.
(20) Golbedaghi, R.; Salehzadeh, S.; Khavasi, H. R.; Blackman, A. G. Mn (II) complexes of three [2+ 2] macrocyclic Schiff base ligands. Synthesis and X-ray crystal structure of the first binuclear-di (binuclear) cocrystal. *Polyhedron* **2014**, *68*, 151−156.
(21) Chou, C.-C.; Su, C.-C.; Tsai, H.-L.; Lii, K.-H. First example of a 2:1 cocrystal of mixed Cu (I)/Cu (II) complexes and a novel ferromagnetic bis (μ-hydroxo) dicopper (II) complex with a bis (pyrazol-1-yl) methane bidentate ligand. *Inorg. Chem.* **2005**, *44* (3), 628−632.
(22) Cherukuvada, S.; Kaur, R.; Guru Row, T. N. Co-crystallization and small molecule crystal form diversity: from pharmaceutical to materials applications. *CrystEngComm* **2016**, *18* (44), 8528−8555.
(23) Sun, L.; Wang, Y.; Yang, F.; Zhang, X.; Hu, W. Cocrystal engineering: a collaborative strategy toward functional materials. *Adv. Mater.* **2019**, *31* (39), 1902328.
(24) Sun, L.; Zhu, W.; Zhang, X.; Li, L.; Dong, H.; Hu, W. Creating organic functional materials beyond chemical bond synthesis by organic cocrystal engineering. *J. Am. Chem. Soc.* **2021**, *143* (46), 19243−19256.
(25) Sonoda, Y.; Goto, M.; Tsuzuki, S.; Tamaoki, N. Fluorinated diphenylpolyenes: Crystal structures and emission properties. *J. Phys. Chem. A* **2007**, *111* (51), 13441−13451.
(26) Yan, D.; Delori, A.; Lloyd, G. O.; Friščić, T.; Day, G. M.; Jones, W.; Lu, J.; Wei, M.; Evans, D. G.; Duan, X. A cocrystal strategy to tune the luminescent properties of stilbene-type organic solid-state materials. *Angew. Chem., Int. Ed.* **2011**, *50* (52), 12483−12486.
(27) Yan, D.; Evans, D. G. Molecular crystalline materials with tunable luminescent properties: from polymorphs to multi-component solids. *Mater. Horiz.* **2014**, *1* (1), 46−57.
(28) Tessler, N. Lasers based on semiconducting organic materials. *Adv. Mater.* **1999**, *11* (5), 363−370.
(29) Huang, Y.; Wang, Z.; Chen, Z.; Zhang, Q. Organic Cocrystals: Beyond Electrical Conductivities and Field-Effect Transistors (FETs). *Angew. Chem., Int. Ed.* **2019**, *58* (29), 9696−9711.
(30) Sun, L.; Zhu, W.; Yang, F.; Li, B.; Ren, X.; Zhang, X.; Hu, W. Molecular cocrystals: design, charge-transfer and optoelectronic functionality. *Phys. Chem. Chem. Phys.* **2018**, *20* (9), 6009−6023.
(31) Morimoto, M.; Irie, M. A diarylethene cocrystal that converts light into mechanical work. *J. Am. Chem. Soc.* **2010**, *132* (40), 14172−14178.

(32) Bolton, O.; Matzger, A. J. Improved stability and smart-material functionality realized in an energetic cocrystal. *Angew. Chem., Int. Ed.* **2011**, *123* (38), 9122−9125.
(33) Cherukuvada, S.; Nangia, A. Eutectics as improved pharmaceutical materials: design, properties and characterization. *ChemComm* **2014**, *50* (8), 906−923.
(34) Thakuria, R.; Delori, A.; Jones, W.; Lipert, M. P.; Roy, L.; Rodríguez-Hornedo, N. Pharmaceutical cocrystals and poorly soluble drugs. *Int. J. Pharm.* **2013**, *453* (1), 101−125.
(35) Kalepu, S.; Nekkanti, V. Insoluble drug delivery strategies: review of recent advances and business prospects. *Acta Pharm. Sin. B* **2015**, *5* (5), 442−453.
(36) Berry, D. J.; Steed, J. W. Pharmaceutical cocrystals, salts and multicomponent systems; intermolecular interactions and property based design. *Adv. Drug Delivery Rev.* **2017**, *117*, 3−24.
(37) Almarsson, O.; Zaworotko, M. J. Crystal engineering of the composition of pharmaceutical phases. Do pharmaceutical co-crystals represent a new path to improved medicines? *ChemComm* **2004**, No. 17, 1889−1896.
(38) Steed, J. W. The role of co-crystals in pharmaceutical design. *Trends Pharmacol. Sci.* **2013**, *34* (3), 185−193.
(39) Bolla, G.; Nangia, A. Pharmaceutical cocrystals: walking the talk. *ChemComm* **2016**, *52* (54), 8342−8360.
(40) Joshi, M.; Roy Choudhury, A. Salts of Amoxapine with Improved Solubility for Enhanced Pharmaceutical Applicability. *ACS omega* **2018**, *3* (2), 2406−2416.
(41) Wong, S. N.; Chen, Y. C. S.; Xuan, B.; Sun, C. C.; Chow, S. F. Cocrystal Engineering of Pharmaceutical Solids: Therapeutic Potentials and Challenges. *CrystEngComm* **2021**, *23*, 7005,
(42) Khalaji, M.; Potrzebowski, M. J.; Dudek, M. K. Virtual cocrystal screening methods as tools to understand the formation of pharmaceutical cocrystals—a case study of linezolid, a wide-range antibacterial drug. *Cryst. Growth Des.* **2021**, *21* (4), 2301−2314.
(43) Cappuccino, C.; Cusack, D.; Flanagan, J.; Harrison, C.; Holohan, C.; Lestari, M.; Walsh, G.; Lusi, M. How Many Cocrystals Are We Missing? Assessing Two Crystal Engineering Approaches to Pharmaceutical Cocrystal Screening. *Cryst. Growth Des.* **2022**, *22* (2), 1390−1397.
(44) Karki, S.; Friščić, T.; Fabian, L.; Laity, P. R.; Day, G. M.; Jones, W. Improving mechanical properties of crystalline solids by cocrystal formation: new compressible forms of paracetamol. *Adv. Mater.* **2009**, *21* (38−39), 3905−3909.
(45) Tan, Y.; Yang, Z.; Wang, H.; Li, H.; Nie, F.; Liu, Y.; Yu, Y. High energy explosive with low sensitivity: A new energetic cocrystal based on CL-20 and 1, 4-DNI. *Cryst. Growth Des.* **2019**, *19* (8), 4476−4482.
(46) Qiao, S.; Wang, J.; Yu, Y.; Liu, Y.; Yang, Z.; Li, H. Two novel TNB energetic cocrystals with low melting point: a potential strategy to construct melt cast explosive carriers. *CrystEngComm* **2022**, *24* (16), 2948−2953.
(47) Landenberger, K. B.; Bolton, O.; Matzger, A. J. Two isostructural explosive cocrystals with significantly different thermodynamic stabilities. *Angew. Chem., Int. Ed.* **2013**, *125* (25), 6596−6599.
(48) Landenberger, K. B.; Matzger, A. J. Cocrystal engineering of a prototype energetic material: supramolecular chemistry of 2, 4, 6-trinitrotoluene. *Cryst. Growth Des.* **2010**, *10* (12), 5341−5347.
(49) Zhang, J.; Jin, B.; Peng, R.; Niu, C.; Xiao, L.; Guo, Z.; Zhang, Q. Novel strategies for synthesizing energetic materials based on BTO with improved performances. *Dalton Trans.* **2019**, *48* (31), 11848−11854.
(50) Liang, F.; Wang, N.; Liu, X.; Lin, Z.; Wu, Y. Co-crystal LiCl·(H 3 C 3 N 3 O 3): a promising solar-blind nonlinear optical crystal with giant nonlinearity from coplanar π-conjugated groups. *ChemComm* **2019**, *55* (44), 6257−6260.
(51) Harada, J.; Ohtani, M.; Takahashi, Y.; Inabe, T. Molecular motion, dielectric response, and phase transition of charge-transfer crystals: acquired dynamic and dielectric properties of polar molecules in crystals. *J. Am. Chem. Soc.* **2015**, *137* (13), 4477−4486.
(52) Harada, J.; Yoneyama, N.; Sato, S.; Takahashi, Y.; Inabe, T. Crystals of Charge-Transfer Complexes with Reorienting Polar Molecules: Dielectric Properties and Order-Disorder Phase Transitions. *Cryst. Growth Des.* **2019**, *19* (1), 291−299.
(53) Xu, Y.; Zu, R.; Yennawar, N. H.; Gopalan, V.; Hickey, R. J. Cocrystalline Polymer Films Exhibiting Second-Order Nonlinear Optical Properties. *ACS Macro Lett.* **2021**, *10* (10), 1216−1222.
(54) Wiscons, R. A.; Goud, N. R.; Damron, J. T.; Matzger, A. J. Room-Temperature Ferroelectricity in an Organic Cocrystal. *Angew. Chem., Int. Ed.* **2018**, *130* (29), 9182−9185.
(55) Narayanan, A.; Cao, D.; Frazer, L.; Tayi, A. S.; Blackburn, A. K.; Sue, A. C.-H.; Ketterson, J. B.; Stoddart, J. F.; Stupp, S. I. Ferroelectric polarization and second harmonic generation in supramolecular cocrystals with two axes of charge-transfer. *J. Am. Chem. Soc.* **2017**, *139* (27), 9186−9191.
(56) Childs, S. L.; Chyall, L. J.; Dunlap, J. T.; Smolenskaya, V. N.; Stahly, B. C.; Stahly, G. P. Crystal engineering approach to forming cocrystals of amine hydrochlorides with organic acids. Molecular complexes of fluoxetine hydrochloride with benzoic, succinic, and fumaric acids. *J. Am. Chem. Soc.* **2004**, *126* (41), 13335−13342.
(57) Bolla, G.; Sarma, B.; Nangia, A. K. Crystal Engineering of Pharmaceutical Cocrystals in the Discovery and Development of Improved Drugs. *Chem. Rev.* **2022**, *122*, 11514.
(58) Koshima, H.; Nagano, M.; Asahi, T. Optical activity induced by helical arrangements of tryptamine and 4-chlorobenzoic acid in their cocrystal. *J. Am. Chem. Soc.* **2005**, *127* (8), 2455−2463.
(59) Kodama, K.; Kobayashi, Y.; Saigo, K. Role of the relative molecular length of the components in ternary inclusion crystals in the chiral recognition and assembly of supramolecular helical architectures. *Cryst. Growth Des.* **2007**, *7* (5), 935−939.
(60) Pal, S.; Nandi, A. K. J. M. Cocrystallization behavior of poly (3-alkylthiophenes): Influence of alkyl chain length and head to tail regioregularity. *Macromolecules* **2003**, *36* (22), 8426−8432.
(61) Mukherjee, P.; Drew, M. G.; Gomez-Garcia, C. J.; Ghosh, A. (Ni2),(Ni3), and (Ni2+ Ni3): a unique example of isolated and cocrystallized Ni2 and Ni3 complexes. *Inorg. Chem.* **2009**, *48* (11), 4817−4827.
(62) Das, L. K.; Biswas, A.; Gomez-Garcia, C. J.; Drew, M. G.; Ghosh, A. Isolation of Two Different Ni2Zn Complexes with an Unprecedented Cocrystal Formed by One of Them and a "Coordination Positional Isomer" of the Other. *Inorg. Chem.* **2014**, *53* (1), 434−445.
(63) Wang, X.-L.; Guo, Z.-C.; Liu, G.-C.; Qu, Y.; Yang, S.; Lin, H.-Y.; Zhang, J.-W. Tuning the lead complexes based on a double 1, 10-phenanthroline derivative with versatile coordination behavior by dicarboxylates: from 0D nano-ring to an unprecedented 0D+ 3D cocrystal. *CrystEngComm* **2013**, *15* (3), 551−559.
(64) Kumar, M.; Kariem, M.; Sheikh, H. N.; Frontera, A.; Seth, S. K.; Jassal, A. K. A series of 3D lanthanide coordination polymers decorated with a rigid 3, 5-pyridinedicarboxylic acid linker: syntheses, structural diversity, DFT study, Hirshfeld surface analysis, luminescence and magnetic properties. *Dalton Trans.* **2018**, *47* (35), 12318−12336.
(65) Kumar, M.; Sheikh, H. N.; Fraconetti, A.; Zareba, J. K.; Sahoo, S. C.; Frontera, A. 2, 5-Furandicarboxylic acid as a linker for lanthanide coordination polymers: The role of heteroaromatic π-π stacking and hydrogen bonding. *New J. Chem.* **2019**, *43* (5), 2179−2195.
(66) Kumar, M.; Wu, L.-H.; Kariem, M.; Franconetti, A.; Sheikh, H. N.; Liu, S.-J.; Sahoo, S. C.; Frontera, A. A series of lanthanide-based metal-organic frameworks derived from furan-2, 5-dicarboxylate and glutarate: structure-corroborated density functional theory study, magnetocaloric effect, slow relaxation of magnetization, and luminescent properties. *Inorg. Chem.* **2019**, *58* (12), 7760−7774.
(67) Kumar, M.; Qiu, C.-Q.; Zareba, J. K.; Frontera, A.; Jassal, A. K.; Sahoo, S. C.; Liu, S.-J.; Sheikh, H. N. Magnetic, luminescence, topological and theoretical studies of structurally diverse supramolecular lanthanide coordination polymers with flexible glutaric acid as a linker. *New J. Chem.* **2019**, *43* (36), 14546−14564.
(68) Chen, P. Y.; Wu, M. Z.; Li, T.; Shi, X. J.; Tian, L.; Liu, Z. Y. Lanthanide Tetranuclear Cage and Mononuclear Cocrystalline Nitronyl Nitroxide Complex with Single-Molecule-Magnet Behavior. *Inorg. Chem.* **2018**, *57* (20), 12466−12470.

https://doi.org/10.1021/acs.cgd.2c01256
Cryst. Growth Des. 2023, 23, 2218−2230

(69) Shukla, P.; Metre, R. K.; Du, M. H.; Kong, X. J.; Das, S. [5× 1+ 1× 1] Hexanuclear lanthanide (III) cocrystal complexes: syntheses, structures, and magnetic properties. *Eur. J. Inorg. Chem.* **2019**, *2019* (16), 2216−2223.
(70) Li, X.-L.; Li, J.; Wang, A.; Liu, C.-M.; Cui, M.; Zhang, Y.-Q. Observation of field-induced single-ion magnet behavior in a mononuclear DyIII complex by co-crystallization of a square-planar CuII complex. *Inorg. Chim. Acta* **2020**, *510*, 119718.
(71) Schmidt, B. M.; Pindwal, A.; Venkatesh, A.; Ellern, A.; Rossini, A. J.; Sadow, A. D. Zwitterionic Trivalent (Alkyl) lanthanide Complexes in Ziegler-Type Butadiene Polymerization. *ACS Catal.* **2019**, *9* (2), 827−838.
(72) Halter, D. P.; Palumbo, C. T.; Ziller, J. W.; Gembicky, M.; Rheingold, A. L.; Evans, W. J.; Meyer, K. Electrocatalytic H2O reduction with f-elements: mechanistic insight and overpotential tuning in a series of lanthanide complexes. *J. Am. Chem. Soc.* **2018**, *140* (7), 2587−2594.
(73) Du, Y.; Jiang, Y.; Sun, T.; Zhao, J.; Huang, B.; Peng, D.; Wang, F. Mechanically excited multicolor luminescence in lanthanide ions. *Adv. Mater.* **2019**, *31* (7), 1807062.
(74) Kovacs, D.; Lu, X.; Meszaros, L. S.; Ott, M.; Andres, J.; Borbas, K. E. Photophysics of coumarin and carbostyril-sensitized luminescent lanthanide complexes: implications for complex design in multiplex detection. *J. Am. Chem. Soc.* **2017**, *139* (16), 5756−5767.
(75) Buenzli, J.-C. G. On the design of highly luminescent lanthanide complexes. *Coord. Chem. Rev.* **2015**, *293*, 19−47.
(76) Martinic, I.; Eliseeva, S. V.; Nguyen, T. N.; Pecoraro, V. L.; Petoud, S. Near-infrared optical imaging of necrotic cells by photostable lanthanide-based metallacrowns. *J. Am. Chem. Soc.* **2017**, *139* (25), 8388−8391.
(77) Hirai, Y.; Nakanishi, T.; Kitagawa, Y.; Fushimi, K.; Seki, T.; Ito, H.; Hasegawa, Y. Luminescent Europium (III) Coordination Zippers Linked with Thiophene-Based Bridges. *Angew. Chem., Int. Ed.* **2016**, *55* (39), 12059−12062.
(78) Bernot, K.; Daiguebonne, C.; Calvez, G.; Suffren, Y.; Guillou, O. A journey in lanthanide coordination chemistry: from evaporable dimers to magnetic materials and luminescent devices. *Acc. Chem. Res.* **2021**, *54* (2), 427−440.
(79) Ashebr, T. G.; Li, H.; Ying, X.; Li, X.-L.; Zhao, C.; Liu, S.; Tang, J. Emerging Trends on Designing High-Performance Dysprosium (III) Single-Molecule Magnets. *ACS Mater. Lett.* **2022**, *4* (2), 307−319.
(80) Zabala-Lekuona, A.; Seco, J. M.; Colacio, E. Single-Molecule Magnets: From Mn12-ac to dysprosium metallocenes, a travel in time. *Coord. Chem. Rev.* **2021**, *441*, 213984.
(81) Marin, R.; Brunet, G.; Murugesu, M. Shining new light on multifunctional lanthanide single-molecule magnets. *Angew. Chem., Int. Ed.* **2021**, *60* (4), 1728−1746.
(82) Long, J.; Guari, Y.; Ferreira, R. A.; Carlos, L. D.; Larionova, J. Recent advances in luminescent lanthanide based Single-Molecule Magnets. *Coord. Chem. Rev.* **2018**, *363*, 57−70.
(83) Feltham, H. L.; Brooker, S. Review of purely 4f and mixed-metal nd-4f single-molecule magnets containing only one lanthanide ion. *Coord. Chem. Rev.* **2014**, *276*, 1−33.
(84) Moreno-Pineda, E.; Wernsdorfer, W. Measuring molecular magnets for quantum technologies. *Nat. Rev. Phys.* **2021**, *3* (9), 645−659.
(85) Das, S.; Dey, A.; Kundu, S.; Biswas, S.; Narayanan, R. S.; Titos-Padilla, S.; Lorusso, G.; Evangelisti, M.; Colacio, E.; Chandrasekhar, V. Decanuclear Ln10 Wheels and Vertex-Shared Spirocyclic Ln_5 Cores: Synthesis, Structure, SMM Behavior, and MCE Properties. *Chem.—Eur. J.* **2015**, *21* (47), 16955−16967.
(86) Kumar, M.; Li, L.-Q.; Zaręba, J. K.; Tashi, L.; Sahoo, S. C.; Nyk, M.; Liu, S.-J.; Sheikh, H. N. Lanthanide contraction in action: structural variations in 13 lanthanide (III) thiophene-2, 5-dicarboxylate coordination polymers (Ln= La-Lu, except Pm and Tm) featuring magnetocaloric effect, slow magnetic relaxation, and luminescence-lifetime-based thermometry. *Cryst. Growth Des* **2020**, *20* (10), 6430−6452.
(87) Sen, C.; Kumar, M.; ul Nisa, Z.; Ashashi, N. A.; Frontera, A.; Sahoo, S. C.; Sheikh, H. N. Coordination polymers of manganese (II), cobalt (II), nickel (II) and cadmium (II) decorated with rigid pyrazine-2, 3-dicarboxylic acid linker: Synthesis, structural diversity, DFT study and magneto-luminescence properties. *Polyhedron* **2020**, *187*, 114629.
(88) Ashashi, N. A.; Kumar, M.; ul Nisa, Z.; Frontera, A.; Sahoo, S. C.; Sheikh, H. N. Solvothermal self assembly of three lanthanide (III)-succinates: Crystal structure, topological analysis and DFT calculations on water channel. *J. Mol. Struct.* **2021**, *1245*, 131094.
(89) Ashashi, N. A.; Kumar, M.; Gomila, R. M.; Frontera, A.; Sheikh, H. N.; Sahoo, S. C. Solvothermal synthesis and crystal structures of two Holmium (III)-5-Hydroxyisophthalate entangled coordination polymers and theoretical studies on the importance of $\pi\cdots\pi$ stacking interactions. *J. Mol. Struct.* **2022**, *1254*, 132329.
(90) Ungur, L.; Chibotaru, L. F. Strategies toward high-temperature lanthanide-based single-molecule magnets. *Inorg. Chem.* **2016**, *55* (20), 10043−10056.
(91) Zhu, Z.; Guo, M.; Li, X.-L.; Tang, J. Molecular magnetism of lanthanide: Advances and perspectives. *Coord. Chem. Rev.* **2019**, *378*, 350−364.
(92) Harriman, K. L.; Brosmer, J. L.; Ungur, L.; Diaconescu, P. L.; Murugesu, M. Pursuit of record breaking energy barriers: a study of magnetic axiality in diamide ligated DyIII single-molecule magnets. *J. Am. Chem. Soc.* **2017**, *139* (4), 1420−1423.
(93) Bar, A. K.; Kalita, P.; Singh, M. K.; Rajaraman, G.; Chandrasekhar, V. Low-coordinate mononuclear lanthanide complexes as molecular nanomagnets. *Coord. Chem. Rev.* **2018**, *367*, 163−216.
(94) Gupta, S. K.; Murugavel, R. Enriching lanthanide single-ion magnetism through symmetry and axiality. *ChemComm* **2018**, *54* (30), 3685−3696.
(95) Norel, L.; Darago, L. E.; Le Guennic, B.; Chakarawet, K.; Gonzalez, M. I.; Olshansky, J. H.; Rigaut, S.; Long, J. R. A terminal fluoride ligand generates axial magnetic anisotropy in dysprosium complexes. *Angew. Chem., Int. Ed.* **2018**, *130* (7), 1951−1956.
(96) Ding, Y. S.; Han, T.; Zhai, Y. Q.; Reta, D.; Chilton, N. F.; Winpenny, R. E.; Zheng, Y. Z. A Study of Magnetic Relaxation in Dysprosium (III) Single-Molecule Magnets. *Chem.—Eur. J.* **2020**, *26* (26), 5893−5902.
(97) Biswas, S.; Bejoymohandas, K. S.; Das, S.; Kalita, P.; Reddy, M. L.; Oyarzabal, I.; Colacio, E.; Chandrasekhar, V. Mononuclear lanthanide complexes: energy-barrier enhancement by ligand substitution in field-induced DyIII SIMs. *Inorg. Chem.* **2017**, *56* (14), 7985−7997.
(98) Biswas, S.; Das, S.; Rogez, G.; Chandrasekhar, V. Hydrazone-Ligand-Based Homodinuclear Lanthanide Complexes: Synthesis, Structure, and Magnetism. *Eur. J. Inorg. Chem.* **2016**, *2016* (20), 3322−3329.
(99) Das, S.; Hossain, S.; Dey, A.; Biswas, S.; Pardo, E.; Lloret, F.; Chandrasekhar, V. Heterometallic Pentanuclear [Ni4Ln](LnIII= Gd, Tb, Dy, Ho) Complexes: Accidental Orthogonality Leading to Ferromagnetic Interactions. *Eur. J. Inorg. Chem.* **2014**, *2014* (21), 3393−3400.
(100) Dey, A.; Kalita, P.; Chandrasekhar, V. Lanthanide (III)-based single-ion magnets. *ACS omega* **2018**, *3* (8), 9462−9475.
(101) Mishra, A.; Wernsdorfer, W.; Abboud, K. A.; Christou, G. Initial observation of magnetization hysteresis and quantum tunneling in mixed manganese- lanthanide single-molecule magnets. *J. Am. Chem. Soc.* **2004**, *126* (48), 15648−15649.
(102) Blagg, R. J.; Ungur, L.; Tuna, F.; Speak, J.; Comar, P.; Collison, D.; Wernsdorfer, W.; McInnes, E. J.; Chibotaru, L. F.; Winpenny, R. E. Magnetic relaxation pathways in lanthanide single-molecule magnets. *Nat. Chem.* **2013**, *5* (8), 673−678.
(103) Ortu, F.; Reta, D.; Ding, Y.-S.; Goodwin, C. A. P.; Gregson, M. P.; McInnes, E. J. L.; Winpenny, R. E. P.; Zheng, Y.-Z.; Liddle, S. T.; Mills, D. P.; Chilton, N. F. Studies of hysteresis and quantum tunnelling of the magnetisation in dysprosium (III) single molecule magnets. *Dalton Trans.* **2019**, *48* (24), 8541−8545.
(104) Mannini, M.; Pineider, F.; Danieli, C.; Totti, F.; Sorace, L.; Sainctavit, P.; Arrio, M.-A.; Otero, E.; Joly, L.; Cezar, J. C.; Cornia, A.;

https://doi.org/10.1021/acs.cgd.2c01256
Cryst. Growth Des. 2023, 23, 2218−2230

Sessoli, R. Quantum tunnelling of the magnetization in a monolayer of oriented single-molecule magnets. *Nature* **2010**, *468* (7322), 417−421.
(105) Das, S.; Hossain, S.; Dey, A.; Biswas, S.; Sutter, J.-P.; Chandrasekhar, V. Molecular magnets based on homometallic hexanuclear lanthanide (III) complexes. *Inorg. Chem.* **2014**, *53* (10), 5020−5028.
(106) Das, S.; Dey, A.; Biswas, S.; Colacio, E.; Chandrasekhar, V. Hydroxide-free cubane-shaped tetranuclear [Ln4] complexes. *Inorg. Chem.* **2014**, *53* (7), 3417−3426.
(107) Canaj, A. B.; Dey, S.; Martí, E. R.; Wilson, C.; Rajaraman, G.; Murrie, M. Insight into D6h Symmetry: Targeting Strong Axiality in Stable Dysprosium (III) Hexagonal Bipyramidal Single-Ion Magnets. *Angew. Chem., Int. Ed.* **2019**, *58* (40), 14146−14151.
(108) Guo, F.-S.; Day, B. M.; Chen, Y.-C.; Tong, M.-L.; Mansikkamäki, A.; Layfield, R. A. Magnetic hysteresis up to 80 K in a dysprosium metallocene single-molecule magnet. *Science* **2018**, *362* (6421), 1400−1403.
(109) Liu, J.-L.; Chen, Y.-C.; Tong, M.-L. Symmetry strategies for high performance lanthanide-based single-molecule magnets. *Chem. Soc. Rev.* **2018**, *47* (7), 2431−2453.
(110) Akhtar, M. N.; AlDamen, M. A.; McMillen, C. D.; Escuer, A.; Mayans, J. Exploring the Role of Intramolecular Interactions in the Suppression of Quantum Tunneling of the Magnetization in a 3d-4f Single-Molecule Magnet. *Inorg. Chem.* **2021**, *60* (13), 9302−9308.
(111) Biswas, S.; Das, S.; Hossain, S.; Bar, A. K.; Sutter, J. P.; Chandrasekhar, V. Tetranuclear Lanthanide (III) Complexes Containing a Square-Grid Core: Synthesis, Structure, and Magnetism. *Eur. J. Inorg. Chem.* **2016**, *2016* (28), 4683−4692.
(112) Biswas, S.; Das, S.; van Leusen, J.; Kögerler, P.; Chandrasekhar, V. Pentanuclear [2.2] spirocyclic lanthanide (III) complexes: slow magnetic relaxation of the Dy III analogue. *Dalton Trans* **2015**, *44* (44), 19282−19293.
(113) Hossain, S.; Das, S.; Chakraborty, A.; Lloret, F.; Cano, J.; Pardo, E.; Chandrasekhar, V. S-shaped decanuclear heterometallic [Ni_8 Ln_2] complexes [Ln^{III}= Gd, Tb, Dy and Ho]: theoretical modeling of the magnetic properties of the gadolinium analogue. *Dalton Trans* **2014**, *43* (26), 10164−10174.
(114) Chandrasekhar, V.; Das, S.; Dey, A.; Hossain, S.; Kundu, S.; Colacio, E. Linear, Edge-Sharing Heterometallic Trinuclear [Co^{II}-Ln^{III}-Co^{II}](Ln^{III}= Gd^{III}, Dy^{III}, Tb^{III}, and Ho^{III}) Complexes: Slow Relaxation of Magnetization in the DyIII Derivative. *Eur. J. Inorg. Chem.* **2014**, *2014* (2), 397−406.
(115) Ashebr, T. G.; Li, H.; Ying, X.; Li, X.-L.; Zhao, C.; Liu, S.; Tang, J. Emerging Trends on Designing High-Performance Dysprosium (III) Single-Molecule Magnets. *ACS Materials Letters* **2022**, *4* (2), 307−319.
(116) Upadhyay, A.; Das, C.; Vaidya, S.; Singh, S. K.; Gupta, T.; Mondol, R.; Langley, S. K.; Murray, K. S.; Rajaraman, G.; Shanmugam, M. Role of the Diamagnetic Zinc (II) Ion in Determining the Electronic Structure of Lanthanide Single-Ion Magnets. *Chem.—Eur. J.* **2017**, *23* (20), 4903−4916.
(117) Boulkedid, A.-L.; Long, J.; Beghidja, C.; Guari, Y.; Beghidja, A.; Larionova, J. A luminescent Schiff-base heterotrinuclear Zn 2 Dy single-molecule magnet with an axial crystal field. *Dalton Trans* **2018**, *47* (5), 1402−1406.
(118) Zhao, Z.-Y.; Xu, H.-H.; Chen, P.; Li, Y.-X.; Sui, Y.; Sun, W.-B. Optimization and expansion of the Schiff base [Zn-Dy] unit to enhance the performance of single molecule magnetic materials. *J. Mater. Chem. C* **2020**, *8* (14), 4843−4850.
(119) Chakraborty, A.; Goura, J.; Kalita, P.; Swain, A.; Rajaraman, G.; Chandrasekhar, V. Heterometallic 3d-4f single molecule magnets containing diamagnetic metal ions. *Dalton Trans* **2018**, *47* (27), 8841−8864.
(120) *SMART & SAINT Software Reference Manuals, Version 6.45*; Bruker Analytical X-ray Systems, Inc; Madison, WI, 2003.
(121) Sheldrick, G. *SADABS, Software for Empirical Absorption Correction*, Ver. 2.05; University of Göttingen: Göttingen, Germany, 2002.
(122) Sheldrick, G. *SHELXTL v. 6.12, Structure Determination Software Suite*; Bruker AXS Madison: Wisconsin, USA, 2000.
(123) Sheldrick, G. M. A short history of SHELX. *Acta Crystallographica Section A: Foundations of Crystallography* **2008**, *64* (1), 112−122.
(124) Sheldrick, G. *SHELXL-2014, Program for the Refinement of Crystal Structures*; University of Göttingen: Germany, 2014.
(125) Dolomanov, O. V.; Bourhis, L. J.; Gildea, R. J.; Howard, J. A.; Puschmann, H. OLEX2: a complete structure solution, refinement and analysis program. *Journal of applied crystallography* **2009**, *42* (2), 339−341.
(126) Bradenburg, K.; Putz, H. *Diamond, version 3.1 e*; Crystal Impact GbR: Bonn, Germany, 2005.
(127) Khan, A.; Akhtar, M. N.; Lan, Y.; Anson, C. E.; Powell, A. K. Linear shaped hetero-metallic [Zn2Ln4] clusters with Schiff base ligand: Synthesis, characterization and magnetic properties. *Inorg. Chim. Acta* **2021**, *524*, 120437.
(128) Wang, H.-L.; Peng, J.-M.; Zhu, Z.-H.; Mo, K.-Q.; Ma, X.-F.; Li, B.; Zou, H.-H.; Liang, F.-P. Step-by-step and competitive assembly of two Dy (III) single-molecule magnets with their performance tuned by Schiff base ligands. *Cryst. Growth Des.* **2019**, *19* (9), 5369−5375.
(129) Patil, S. A.; Weng, C.-M.; Huang, P.-C.; Hong, F.-E. Convenient and efficient Suzuki-Miyaura cross-coupling reactions catalyzed by palladium complexes containing N, N, O-tridentate ligands. *Tetrahedron* **2009**, *65* (15), 2889−2897.
(130) Hui, R.-H.; Zhou, P.; You, Z.-L. Crystal structures of two dinuclear cadmium (II) complexes with Schiff bases as ligands. *J. Struct. Chem.* **2010**, *51*, 1201−1204.
(131) Ramakant, G. A.; Ahmed, N.; Tarannum, I.; Mehta, S.; Nandeshwar, M.; Mondal, A.; Singh, S. K.; Prabusankar, G. Ln (III)(Ln= La, Gd, and Dy) Benzimidazolium Tricarboxylate Coordination Polymers with Hydrogen Bonding Modulated Magnetic Relaxation. *Cryst. Growth Des* **2022**, *22*, 6046.
(132) Yesilbağ, S.; Çınar, E. B.; Dege, N.; Ağar, E.; Saif, E. Crystal structure and Hirshfeld surface analysis of dimethyl 3, 3′-{[(1E, 2E)-ethane-1, 2-diylidene] bis (azanylylidene)} bis (4-methylbenzoate). *Acta Crystallogr. E: Crystallogr. Commun.* **2022**, *78* (4), 340.
(133) Yin, C.-L.; Hu, Z.-B.; Long, Q.-Q.; Wang, H.-S.; Li, J.; Song, Y.; Zhang, Z.-C.; Zhang, Y.-Q.; Pan, Z.-Q. Single molecule magnet behaviors of Zn 4 Ln 2 (Ln= Dy III, Tb III) complexes with multidentate organic ligands formed by absorption of CO 2 in air through in situ reactions. *Dalton Trans* **2019**, *48* (2), 512−522.
(134) Roy, S.; Shukla, P.; Kumar, R.; Sahoo, S. C.; Pal, T. K.; Rajput, A.; Klak, J.; Hada, M.; Vignesh, K. R.; Das, S. Utilization of diamagnetic Zn (II) ion to boost the anisotropic nature of Ln (III) ion in heterodinuclear Zn (II)-Ln (III) SMMs. *Appl. Organomet. Chem.* **2022**, *36*, No. e6914.
(135) Das, S.; Bejoymohandas, K.; Dey, A.; Biswas, S.; Reddy, M.; Morales, R.; Ruiz, E.; Titos-Padilla, S.; Colacio, E.; Chandrasekhar, V. Amending the Anisotropy Barrier and Luminescence Behavior of Heterometallic Trinuclear Linear [MII−LnIII−MII](LnIII= Gd, Tb, Dy; MII= Mg/Zn) Complexes by Change from Divalent Paramagnetic to Diamagnetic Metal Ions. *Chem.—Eur. J.* **2015**, *21* (17), 6449−6464.
(136) Ghosh, T. K.; Maity, S.; Mayans, J.; Ghosh, A. Family of isomeric CuII-LnIII (Ln= Gd, Tb, and Dy) complexes presenting field-induced slow relaxation of magnetization only for the members containing GdIII. *Inorg. Chem.* **2021**, *60* (1), 438−448.
(137) Zhang, S.; Mo, W.; Zhang, J.; Zhang, Z.; Yin, B.; Hu, D.; Chen, S. Regulation of substituent effects on configurations and magnetic performances of mononuclear DyIII single-molecule magnets. *Inorg. Chem.* **2019**, *58* (22), 15330−15343.
(138) Sun, L.; Zhang, S.; Jiang, Z.; Yang, Q.; Chen, S.; Zhang, Y.; Wang, W.; Wei, Q.; Xie, G. Interchange between coordinated and lattice solvents generates the highest energy barrier within nine-coordinated Dy III single molecule magnets. *Dalton Trans* **2017**, *46* (34), 11159−11165.
(139) Liu, C.-M.; Sun, R.; Wang, B.-W.; Wu, F.; Hao, X.; Shen, Z. Homochiral Ferromagnetic Coupling Dy2 Single-Molecule Magnets with Strong Magneto-Optical Faraday Effects at Room Temperature. *Inorg. Chem.* **2021**, *60* (16), 12039−12048.

https://doi.org/10.1021/acs.cgd.2c01256
Cryst. Growth Des. 2023, 23, 2218−2230